ChemCatChem

The European Society Journal for Catalysis

Chemistry Europe

European Chemical Societies Publishing

Supported by GECATS GERMAN CATALYSIS SOCIETY

Accepted Article

Title: TiO2@UiO-66 Composites with Efficient Adsorption and Photocatalytic Oxidation of VOCs: Investigation of Synergistic Effect and Reaction Mechanism

Authors: Jinhui Zhang, Ziyang Guo, Zhenxiang Yang, Jun Wang, Jun Xie, Mingli Fu, and Yun Hu

To be cited as: *ChemCatChem* 10.1002/cctc.202001466

Link to VoR: https://doi.org/10.1002/cctc.202001466

WILEY-VCH

FULL PAPER WILEY-VCH

TiO_2@UiO-66 Composites with Efficient Adsorption and Photocatalytic Oxidation of VOCs: Investigation of Synergistic Effect and Reaction Mechanism

Jinhui Zhang,[a] Ziyang Guo,[a] Zhenxiang Yang,[a] Jun Wang,[a] Jun Xie,[a] Mingli Fu,[a,b,c] Yun Hu*[a,b,c]

[a] J. Zhang, Z. Guo, Z. Yang, J. Wang, J. Xie, Prof. M. Fu, Prof. Y. Hu*
School of Environment and Energy
South China University of Technology
Guangzhou Higher Education Mega Centre, Guangzhou 510006 (P.R. China)
*E-mail: huyun@scut.edu.cn
[b] Prof. M. Fu, Prof. Y. Hu
Guangdong Provincial Key Laboratory of Atmospheric Environment and Pollution Control
South China University of Technology
Guangzhou Higher Education Mega Centre, Guangzhou 510006 (P.R. China)
[c] Prof. M. Fu, Prof. Y. Hu
Guangdong Provincial Engineering and Technology Research Centre for Environmental Risk Prevention and Emergency Disposal
South China University of Technology
Guangzhou Higher Education Mega Centre, Guangzhou 510006 (P.R. China)

Supporting information for this article is given via a link at the end of the document.

Abstract: TiO_2@UiO-66 composite with intimate contact interfaces is fabricated by in situ solvothermal methods. Compared with other UiO-based composites, TiO_2@UiO-66 exhibits superior photocatalytic activity for oxidation of toluene into CO_2 during long-time reaction under flowing conditions. This is because (1) the intimate contact interface and well-matched band structure between TiO_2 and UiO-66 can effectively separate and transfer photogenerated electrons; (2) the synergistic effect between UiO-66 and TiO_2 promotes the adsorption of toluene and desorption of CO_2 and provides sufficient active sites for photocatalytic reaction. The toluene conversion and CO_2 production on 4TiO_2@U are 3.27 and 4.10 times higher than that on UiO-66, respectively. 4TiO_2@U also shows the highest activity for formaldehyde and Rhodamine B degradations. The in situ FTIR results exhibit that toluene can be oxidized by $\bullet O_2^-$ and h^+ to benzaldehyde and benzoic acid, then further oxidized to oxalic acid, and finally mineralized into CO_2 and H_2O.

1. Introduction

Volatile organic compounds (VOCs) are considered as a kind of toxic pollutants in the atmosphere, which are mainly from building materials, furniture, decoration materials and other consumer products.[1,2] They not only give rise to a harmful effect on human health but also lead to serious ecosystem effects.[3,4] Semiconductor photocatalysis has been proved to be an effective and promising alternative technology for the removal of VOCs from the atmospheric environment under mild operating conditions.[5-7]

TiO_2 is the most common photocatalyst in environmental remediation because of its strong oxidative ability, low environmental influence, low cost and chemical stability.[8,9] However, the rapid recombination of photoinduced carriers limits the wide applications of TiO_2. Therefore, numerous studies have been carried out to solve this problem, such as ions doping[10], surface modification[11] and semiconductor coupling[9,12]. Among them, semiconductor coupling is an efficient method to achieve superior photocatalytic performance due to the effective separation and transfer of photoinduced electrons-holes. Therefore, various TiO_2 based heterojunctions including WO_3/TiO_2,[13] Pt-MoS_2/TiO_2,[14] CuS-CdS/TiO_2,[15] and $LaVO_4/TiO_2$[16] have drawn much attention due to their good photocatalytic performance for toluene degradation. However, the activity and mineralization efficiency dramatically dropped after several static cycles or long-term flowing condition evaluation due to the carbonaceous residues during the reaction. Therefore, to explore of TiO_2-based composites with stable and high photocatalytic activity and CO_2 selectivity during long-term VOCs degradation is imperative.

Metal-organic frameworks (MOFs) are a fascinating class of porous crystalline materials built by joining the metal-oxo clusters with organic linker. MOFs have drawn extensive attention due to the tunable pore size, large surface area, pore volumes and designable framework structures.[17] Based on these characteristics, MOFs have attracted great study in many fields, such as gas storage,[18] separation[19] and catalysis[20]. Meanwhile, MOFs have been used in photocatalytic oxidation of VOCs as photocatalysts and exhibit some photocatalytic activity.[21-23] TiO_2-UiO-66-NH_2 composite was synthesized and used for VOCs degradation under flowing conditions. The composite exhibited good VOCs conversion while the CO_2 selectivity is poor.[21-22] MIL-101-Fe-NH_2 was synthesized by Zhang et al. and used for toluene degradation under static conditions. It was found that the sample had a good toluene removal rate, but it took 10 h to reach the degradation rate of 79.8%.[23] Additionally, the strength of the interaction between MOF and toluene or CO_2 was not considered, and some researches have pointed out that MOF with -NH_2 is not an ideal MOF candidate material for VOCs degradation because -NH_2 has strong adsorption performance for CO_2 molecule.[24-26] Moreover, the possible reaction mechanism of toluene on MOF based composite under dynamic reaction system has not been explored. Therefore, we have designed a high-performance MOF based composite by in situ synthesis method for the first time for VOCs degradation under flowing conditions, and explored the role of MOFs in the VOCs oxidation process.

Herein, a series of TiO_2@UiO-66 composite is fabricated via in situ solvothermal approach and the photocatalytic performance of the composite was investigated by VOCs oxidation under UV condition. UiO-66 is a typical Zr-based MOF material, which has a similar topological structure with UiO-66-NH_2, with regular 3D structure, high surface area, excellent stability and semiconductor properties. The TiO_2@UiO-66 composite showed superior and stable photocatalytic activity and CO_2 selectivity for toluene degradation during long-term evaluation under flowing condition, compared to pure TiO_2, UiO-66 and TiO_2-UiO-66 prepared by evaporation (named as: 4TiO_2-U-Evap) and mechanical (named as: 4TiO_2-U-Mech) methods. The intimate contact interfaces between TiO_2 and UiO-66 in the TiO_2@UiO-66 composite promoted the separation and the transfer of photoinduced charge carriers. Meanwhile, the synergistic effect of the adsorption capacity of the MOF and the photocatalytic properties of TiO_2 for toluene significantly enhanced the removal efficiency. Such a method of exploring the role of MOF in toluene photocatalytic oxidation provided a theoretical foundation for the design of high-performance MOF based photocatalysts for VOCs degradation.

2. Results and Discussion

2.1 Characterization of photocatalysts

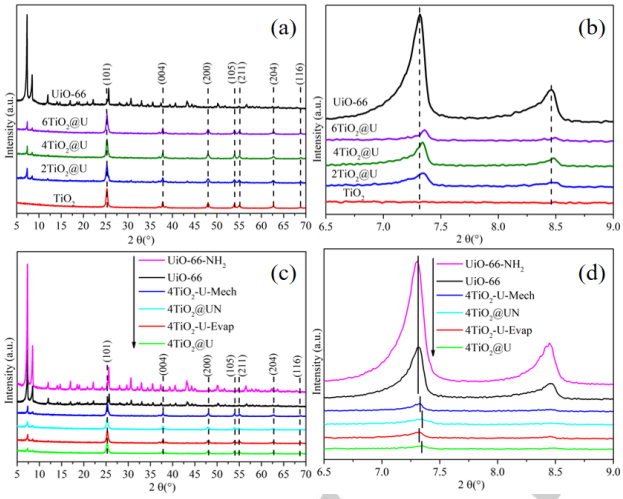

Figure 1. XRD patterns (a,c) and enlarged view (b,d) of the different composites.

XRD analysis is used to determine the crystallite structure and the composition of composites. The diffraction of UiO-66 is perfectly in agreement with that reported in the literature (Figure 1a),[27] demonstrating UiO-66 has been successfully synthesized. In the case of TiO_2, only anatase phase is detected (JCPDS 021-1272). For the TiO_2@UiO-66 composite, all peaks in composite can be attributed to those of UiO-66 and TiO_2, indicating that the composite is successfully synthesized. Meanwhile, the XRD peaks of TiO_2@UiO-66 composite exhibit an obvious right-shift compared to pure UiO-66 (Figure 1b). The right-shift of XRD peaks is may be because the hard oxophilic Zr^{4+} (preferential pre-coordination with soft oxygen groups of the TiO_2 based on the hard-soft acid-base principle) and H_2BDC in situ self-assembly around the TiO_2 under a high temperature to form TiO_2@UiO-66.[22,28] Therefore, the strong phase interactions exist between TiO_2 and UiO-66 based on the XRD results. In addition, UiO-66-NH_2, 4TiO_2-U-Mech, 4TiO_2-U-Evap and 4TiO_2@UN have been all successfully prepared. They also have phase interactions exist between two components in the composite (Figure 1c and 1d). However, compared with the composite prepared by evaporation and mechanical methods (Figure 1d), the diffraction peak of 4TiO_2@U prepared by in situ method shifts to a higher large-angle side, suggesting a stronger interaction between two components in the composite prepared by in situ solvothermal method.

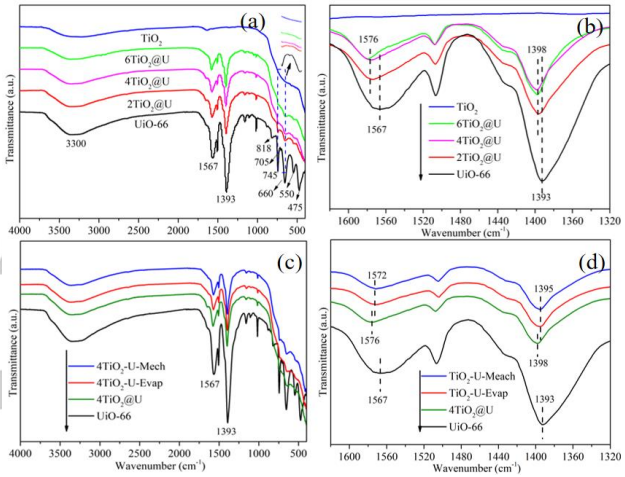

Figure 2. FT-IR spectra (a,c) and enlarged view (b,d) of the different composites.

The FT-IR spectra are performed to illustrate the molecular structure of the samples. In Figure 2a, the broad peak located around 3000-3700 cm^{-1} is ascribed to the O-H stretching band of water molecules on the samples. The broad peak attributed to Ti-O-Ti stretching vibration is observed on TiO_2 at the range of 400-900 cm^{-1}. The band at 1638 cm^{-1} is assigned to hydroxyl stretching vibration resulting from the Ti-OH bond on the TiO_2 surface. As for UiO-66, the bands at 1567 and 1393 cm^{-1} are assigned to the asymmetric and symmetric vibration of carboxyl groups in the benzene rings of UiO-66, respectively.[29] In addition, the peaks at 818 and 745 cm^{-1} are the C-H vibration and O-H vibration in terephthalate ligand, respectively.[29,30] The band at 550 cm^{-1} is related to the Zr-(OC) asymmetric stretching vibration.[30] The peaks at 660 and 475 cm^{-1} are assigned to the μ_3-O and the μ_3-OH stretching vibration, respectively.[30,31] Compared with the pristine UiO-66, the relative intensity of UiO-66 characteristic peaks in TiO_2@UiO-66 significantly decreases, and the characteristic peak of TiO_2 increases. It is worth noting that the IR band ~705 gradually appeared and increased with increase TiO_2 content (see inset enlarged view in Figure 2a), suggesting that the generation of Ti-O-Zr groups.[32] The new characteristic peak indicated that the TiO_2 successfully coordinated with Zr^{4+} cations, forming tight interfacial contact between TiO_2 and UiO-66.[22] Furthermore, from the narrow scan spectra (Figure 2b), the symmetric Vs(COO-) and asymmetric

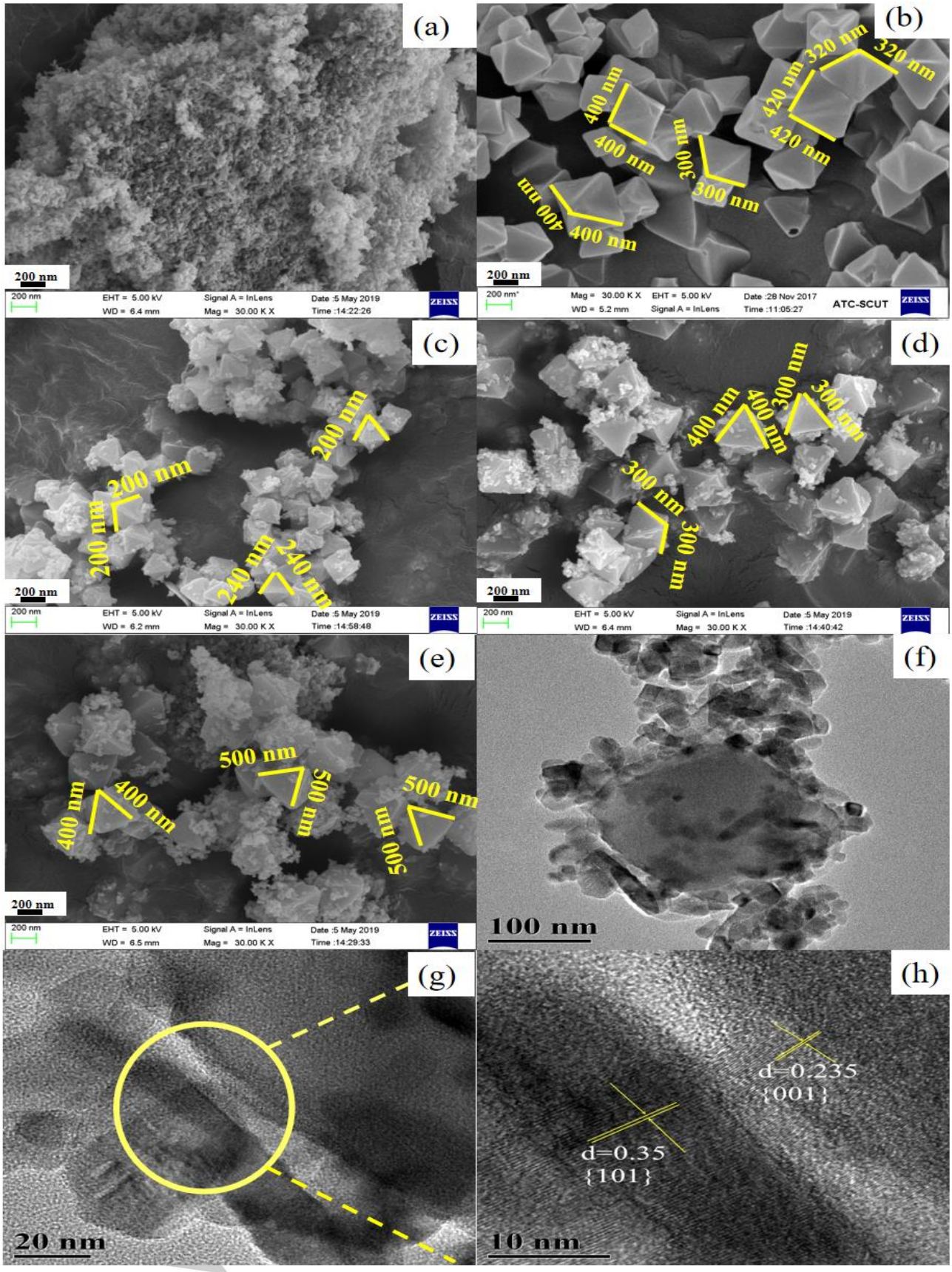

Figure 3. SEM images of TiO_2 (a), UiO-66 (b), $2TiO_2$@U (c), $4TiO_2$@U (d), $6TiO_2$@U (e) and TEM images of $4TiO_2$@U (f, g and h).

Vas(COO^-) vibration of carboxyl groups in the ligand of MOFs slightly shift from 1393 and 1567 cm^{-1} to 1398 and 1576 cm^{-1} respectively, with increasing TiO_2 content. This suggests that the chemical environment around UiO-66 has been changed, because the UiO-66 crystals grow in situ in the presence of the TiO_2 nanoparticle. Besides, the IR data show that UiO-66-NH_2, 4TiO_2@UN, 4TiO_2-U-Mech and 4TiO_2-U-Evap have been successfully prepared. Meanwhile, there are also interactions between the two components in the composite (Figure 2c, 2d and Figure S1) because the carboxyl groups in the ligand of MOFs slightly shift to higher wavenumber. However, compared with 4TiO_2-U-Mech and 4TiO_2-U-Evap, the carboxyl groups of 4TiO_2@U shift to a higher wavenumber, indicating that TiO_2 and UiO-66 in 4TiO_2@U have a stronger interaction, which is in accordance with XRD results.

The thermal stability of the composite is analyzed with 4TiO_2@U as a representative material and the result is shown in Figure S2. The Thermo-gravimetric (TG) results of pure UiO-66 exhibits three weight loss, which can be corresponded to the removal of water molecules from surface (below 150 °C), guest molecules decomposition (200-400 °C) and the BDC unit decomposition of UiO-66 (500-600 °C), respectively.[31,33] However, 4TiO_2@U has almost no weight loss below 500 °C, showing a significantly enhanced thermal stability compared to UiO-66. This may be due to the stronger interaction between TiO_2 and UiO-66 which prevents the decomposition of UiO-66. Based on the TG results, the actual contents of TiO_2 and UiO-66 in 4TiO_2@U are 84% and 16%, respectively.[21]

The size, morphology and crystallinity of the as-prepared samples are observed by the SEM and TEM analyses. Pure TiO_2 consists of a large number of small nanoparticles aggregated together (Figure 3a). As shown in Figure 3b, pristine UiO-66 exhibits uniform octahedral structure and clean surface with grain sizes of the edge are about 400 nm. As for TiO_2@UiO-66 composite, TiO_2 is attached to the surface of UiO-66, which is conducive to promote the contact between active sites and VOCs molecules as well as light harvesting in the photocatalytic reaction (Figure 3c-g). Besides, the edge of UiO-66 in composite gradually increases from ca. 200 nm to 500 nm with the increase of the TiO_2 ratio (Figure 3c-e), indicating that strong interactions exist between TiO_2 and UiO-66 of the composite. Meanwhile, the TiO_2 nanoparticles are intimately adhering on the surface of UiO-66 (Figure 3f and g), and the lattice spacing is ca. 0.35 and 0.235 nm, corresponding to the {101} and {001} planes of anatase TiO_2, respectively.

The chemical composition and valence state in TiO_2, UiO-66, 4TiO_2@U, 4TiO_2@UN, 4TiO_2-U-Evap and 4TiO_2@U-Mech are obtained by XPS analyses. XPS survey spectra (Figure S3 and Table S1) indicates that TiO_2-UiO composite is made up of C, N, O, Zr and Ti elements, indicating a two-phase composition of the materials. For UiO-66, the fitted peaks of C 1s at 284.50, 285.11 and 288.80 eV are assigned to the C=C bond, C-H bond and the carboxylate (O-C=O) carbon, respectively (Figure 4a).[33] The peaks of O 1s at 530.46, 531.54 and 532.27 eV can be assigned to the Zr-O bond, C=O in H_2BDC and hydroxyl groups, respectively (Figure 4b).[29] The Zr 3d (Figure 4c) core level spectrum exhibits four peaks, which can be attributed to the Zr $3d_{5/2}$ (182.56 and 183.21 eV) and Zr $3d_{3/2}$ (185.06 and 185.65 eV), respectively, suggesting the existence of Zr^{+4}.[29] In the case of 4TiO_2@U, the binding energy of C 1s is 0.05 eV higher than that of UiO-66 sample. In contrast, the peaks of O 1s and Zr 3d present a significant negative shift of -1.52 and -0.09 eV respectively, as compared with the UiO-66 sample. These results suggest that the surrounding chemical environment of UiO-66 is changed after the introduction of TiO_2. In addition, the characteristic peaks of Ti 2p in the 4TiO_2@U composite (458.55 and 464.60 eV) is 0.35 eV higher than that in TiO_2 (458.45 and 464.25 eV),[34] indicating the existence of an interaction between TiO_2 and UiO-66.

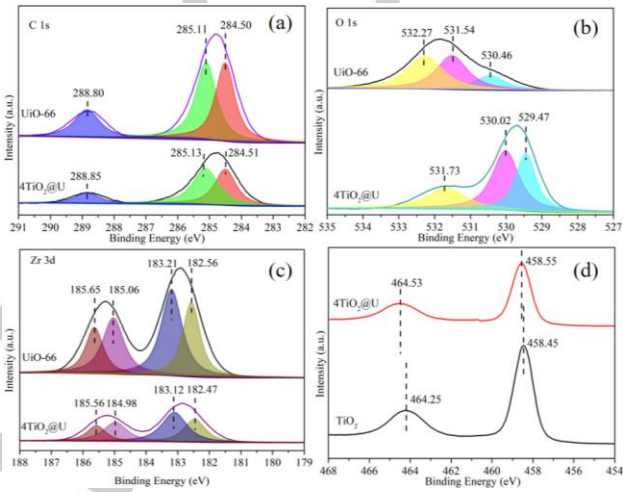

Figure 4. XPS spectra of TiO_2, UiO-66 and 4TiO_2@U: C 1s (a), O 1s (b), Zr 3d (c) and Ti 2p (d).

The XPS results of 4TiO_2-U-Mech, 4TiO_2-U-Evap and 4TiO_2@UN are also investigated (Figure S4 and Figure S5). Compared with 4TiO_2-U-Evap and 4TiO_2-U-Mech, the peaks of Zr 3d in 4TiO_2@U shift to lower binding energy, but the Ti 2p shift to a higher value, indicating the electron density of TiO_2 in 4TiO_2@U shift to Zr more easily. Therefore, it can be concluded that TiO_2 and UiO-66 in 4TiO_2@U prepared by one-pot solvothermal method have a stronger interactions and closer interface contact.

2.2. Photoelectrochemical properties

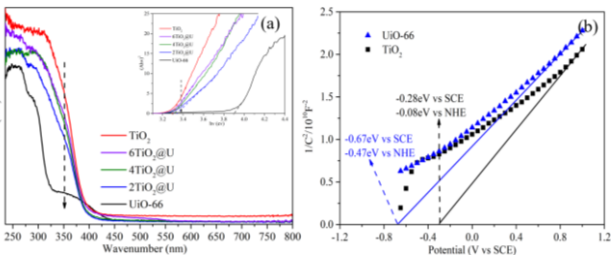

Figure 5. UV-vis absorption spectra and calculated Tauc plot (inset) (a) and Mott-Schottky plot (b) of TiO_2, UiO-66 and TiO_2@UiO-66 composites.

UV-vis absorption spectra of pure TiO_2, UiO-66 and TiO_2-UiO composite are measured to evaluate the optical absorption property. As shown in Figure 5a, compared with the pristine UiO-66, the UV light region absorption intensity of TiO_2@UiO-66 is obviously enhanced as the amount of TiO_2 increases, which can be attributed to the excellent interfacial contact between the TiO_2 and UiO-66. Meanwhile, the absorption intensity of $4TiO_2$@U is higher than that of $4TiO_2$-U-Mech and $4TiO_2$-U-Evap (Figure S6). This is expected to improve the photocatalytic performance of the TiO_2@UiO-66 composite for VOCs degradation.[35] Correspondingly, the band gap energy (E_g) of samples can be calculated by the Kubelka-Munke equation. The Tauc plot (the inset figure in Figure 5a) demonstrates the E_g of TiO_2@UiO-66 composite situates exist between TiO_2 and UiO-66, indicating the strong interaction of the composite structure and the generation of heterojunction between TiO_2 and UiO-66.

To further clarify the electronic structure of the catalysts, the electrochemical flat potential has been measured by using Mott-Schottky plots at the frequency of 1000 Hz. The slopes of all samples are positive, indicating their typical n-type semiconductor nature (Figure 5b). The flat band position of TiO_2 and UiO-66 is -0.08 and -0.47 eV vs NHE, respectively. The conduction band potential (E_{CB}) of n-type semiconductor is 0.2 eV above the flat band potential.[29] Thus, the E_{CB} of TiO_2 and UiO-66 is estimated to be -0.28 and -0.67 eV, respectively. Combined with E_g results and the formula of $E_g=E_{VB}-E_{CB}$, the valence band position (E_{VB}) of TiO_2 and UiO-66 is 3.01 and 3.23 eV, respectively.

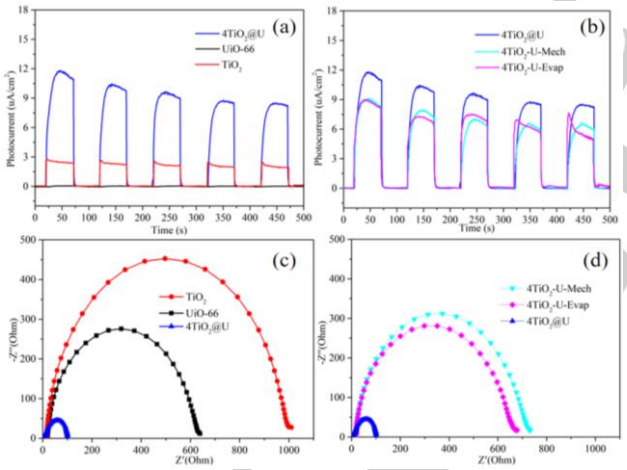

Figure 6. Photocurrent responses (a,b) and EIS Nyquist plots (c,d) of the different composites.

To unveil the charge migration and transfer efficiency in composite, photocurrent analyses are performed and the results are illustrated in Figure 6. Compared with pure TiO_2 and UiO-66, $4TiO_2$@U exhibits superior photocurrents intensity (Figure 6a), indicating that the two components in the composite promote the separation of the photogenerated carrier. $4TiO_2$@U also exhibits a higher photocurrent response than $4TiO_2$-U-Evap and $4TiO_2$-U-Mech, suggesting that a compact connection between the two components can promote separation and transfer efficiency of photoexcited electron-hole (Figure 6b).[9] From the EIS results displayed in Figure 6c and 6d, it can be seen that $4TiO_2$@U also exhibits the highest charge carrier transfer efficiency due to its lowest arc radius, indicating that a "nanoscale mixing" by one-pot solvent-thermal synthesis method will promote electron transfer.

2.3. Photocatalytic performance

2.3.1. Toluene removal and CO_2 production

The photocatalytic activity of TiO_2, UiO-66 and TiO_2@UiO-66 composite is evaluated by oxidation of toluene during long time reaction under UV condition. The sag curves in the first 180 min are attributed to the toluene adsorption/desorption process on the catalyst surfaces (Figure 7a). Under the UV light condition, the toluene concentration exhibits a sudden decrease and then to be stable, especially when toluene passed through the TiO_2@UiO-66 composite. The pristine UiO-66 and TiO_2 show certain photocatalytic activity with only 20.37% and 36.89% of toluene removal respectively, in 720 min, which can be attributed to the rapid recombination of photogenerated carriers. Compared with a single material, the TiO_2@UiO-66 composite exhibits excellent photocatalytic activity, and the highest efficiency is obtained by $4TiO_2$@U, on which 66.59% of toluene is removed within 720 min under UV light irradiation. Also, $4TiO_2$@U shows the highest CO_2 production (103.92 ppm) and selectivity (89%), which is much higher than that of TiO_2 (62.13 ppm) and UiO-66 (25.34 ppm). Thus, it can be found that the $4TiO_2$@U sample shows superior toluene conversion and CO_2 production, which are 3.27 and 4.10 times higher than that of UiO-66 as well as 1.81 and 1.67 times higher than that of pure TiO_2, respectively. These results illustrate that the TiO_2@UiO-66 prepared by in situ solvothermal methods are able to promote the separation and transfer of photoinduced carriers, thus improving the photocatalytic performance.

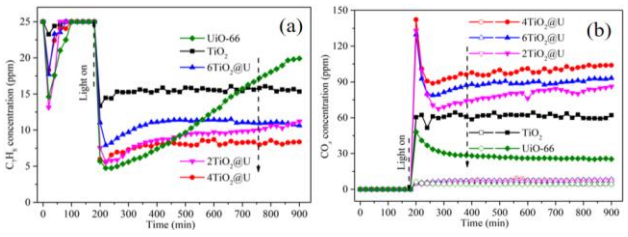

Figure 7. Toluene removal (a) and generated CO_x concentration (b) on the catalysts under UV light irradiation. The close symbols represent [CO_2] and the open symbols represent [CO].

To prove the superiority of UiO-66 over other common UiO topology materials such as UiO-66-NH_2, TiO_2@UiO-66-NH_2 composite is used for toluene degradation under the same condition. As shown in Figure S7, $4TiO_2$@U exhibits higher photocatalytic activity and CO_2 production than $4TiO_2$@UN. This is because amino groups in the porous structure of UiO-66-NH_2 served as basic sites for adsorbing CO_2 molecule, which inhibits the contact of toluene with the active sites.[26,36]

2.3.2. Toluene and formaldehyde degradation on different composites

The photocatalytic oxidation of toluene by $4TiO_2$-U-Mech and $4TiO_2$-U-Evap are also performed under the same reaction condition (Figure 8). $4TiO_2$@U shows higher photocatalytic performance than $4TiO_2$-U-Mech and $4TiO_2$-U-Evap, suggesting the in situ prepared material can more easily promote migration and separation of photogenerated charge carriers because of the intimate connection between the two components. Also, the photocatalytic oxidation of formaldehyde has been carried out (Figure S8). $4TiO_2$@U shows the highest formaldehyde conversion, which is 83% within 72 h of light irradiation. Moreover, the CO_2 selectivity on $4TiO_2$@U reaches 90%. We also compared our work with some relevant researches. The composites and reaction system in this study exhibit higher photocatalytic activity and selectivity even under more difficult reaction conditions (Table S2).

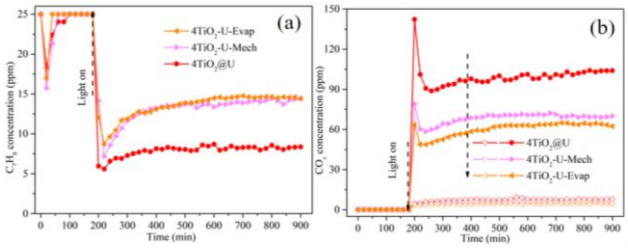

Figure 8. Toluene removal (a) and generated CO_x concentration (b) on different composites under UV light irradiation. The close symbols represent [CO_2] and the open symbols represent [CO].

2.3.3. Photocatalytic degradation of RhB

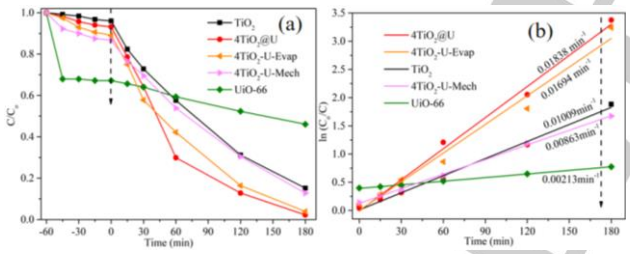

Figure 9. Photocatalytic degradation of RhB (a) and linear fit log plots of RhB (b) degradation curves by different photocatalysts under UV light irradiation.

In order to fully evaluate the photocatalytic performance of the composite, photocatalytic degradation of RhB in wastewater is carried out under the UV light conditions. Compared with pure TiO_2, UiO-66, $4TiO_2$-U-Mech and $4TiO_2$-U-Evap, $4TiO_2$@U shows the highest photocatalytic activity, the removal efficiency of RhB is 97.58% in 180 min (Figure 9a). These results indicate that the composite prepared by in situ solvothermal method can promote the charge carrier separation, thus improving the photocatalytic activity. A pseudo-first order kinetic equation [$-\ln(C/C_o) = kt$] produces a good fit to the experimental data (Figure 9b). The reaction rate constant k of $4TiO_2$@U is 0.01838 min^{-1}, which is about 1.82 and 8.63 times higher than that of TiO_2 (0.01009 min^{-1}) and UiO-66 (0.00213 min^{-1}), respectively. Both liquid phase and gas phase reactions show that $4TiO_2$@U can be widely used in water treatment and air pollution control.

2.3.4. Effects of humidity

To investigate the effect of relative humidity (RH) on toluene removal over $4TiO_2$@U material, the oxidation reactions of toluene with different relative humidity levels (RH=0% (extreme dry), 20% (dry), 40% (dry) and 60% (moderate), 80% (humid)) have been performed and the results are shown in Figure 10. When the RH increases from 0% to 20%, the adsorption amount of toluene is similar, indicating that relative dry condition has little effect on the adsorption of toluene. However, the adsorption amount of toluene significantly decreases when the RH increases from 20% to 80%, suggesting that a high water vapor level in the air stream can generate a well-organized physical barrier on the material surface and impede effective contact between pollutant and catalyst surface.[37] Under the UV light condition, it can be found that the photocatalytic performance of $4TiO_2$@U also depends on the RH. As the RH increases from 0 to 80%, the toluene removal and CO_2 production initially increases and then decreases, reaching a maximum performance at RH=60%. According to previous study,[37,38] water vapor can generate hydroxyl radical (• OH) served as active species during the photocatalytic process. Meanwhile, a research has pointed out that the competitive adsorption of water molecules and reaction intermediates on the photocatalyst surface can prevent the deactivation of the catalyst.[39] Thus, it can be concluded that water molecules both have a negative effect on the adsorption process and a positive effect on the photocatalysis process.

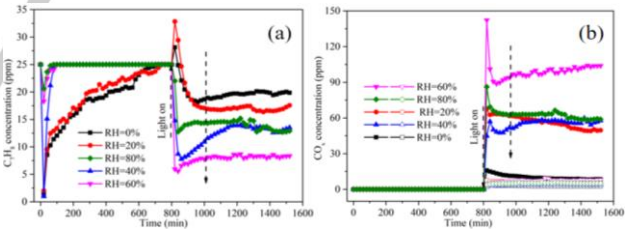

Figure 10. Toluene removal (a) and generated CO_x concentration (b) by $4TiO_2$@U under different relative humidity. The close symbols represent [CO_2] and the open symbols represent [CO].

To further investigate the effect of RH on adsorption and photocatalysis process, the photocatalytic degradation of toluene by $4TiO_2$@U has been performed at 60% or 0% RH and under the dark or illumination conditions, respectively (Figure S9). It can be found that water molecules not only occupy active sites under dark conditions and inhibit the adsorption of toluene, but also can promote the degradation of toluene under UV light irradiation. This clearly indicates that appropriate RH plays a key role in photocatalytic reaction.

2.3.5. Catalyst stability

To verify the stability of the composite under UV light irradiation, $4TiO_2$@U has been characterized before and after photoreaction using XRD and SEM analyses. The crystalline structure of the fresh and used composites are similar after 720 min irradiation (Figure S10a). In addition, no apparent changes in morphology structure are observed before and after the reaction (Figure S10b and 10c). These results demonstrate that the as-prepared $4TiO_2$@U composite has high stability during the photocatalytic oxidation process.

2.4 Mechanism for toluene photocatalytic oxidation

2.4.1 Temperature programmed desorption

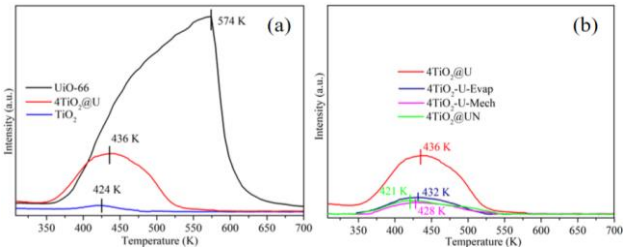

Figure 11. Toluene-TPD profiles of different samples: (a) UiO-66, TiO_2 and $4TiO_2$@U, (b) $4TiO_2$@U, $4TiO_2$-U-Evap, $4TiO_2$-U-Mech and $4TiO_2$@UN.

The C_7H_8-TPD tests are used to provide an insight into the interaction between toluene and samples. As shown in Figure 11a and Table 1, pure TiO_2 shows poor toluene adsorption capacity due to its low surface area and non-porous structure. In contrast, due to the high surface area and 3D porous structure, pristine UiO-66 exhibits excellent toluene adsorption capacity. As for $4TiO_2$@U, the toluene adsorption capacity is higher than that of TiO_2, but lower than that of UiO-66, indicating that UiO-66 in the composite is the main site for toluene adsorption. Meanwhile, the desorption peak temperature of toluene on UiO-66 is higher than that of pure TiO_2, suggesting the interaction of toluene with UiO-66 is stronger than that with TiO_2. For $4TiO_2$@U composite, the desorption peak temperature of toluene is between pure TiO_2 and UiO-66, indicating that the interaction between $4TiO_2$@U and toluene is mainly originated from UiO-66. Additionally, compared with TiO_2 and UiO-66, $4TiO_2$@U composite exhibits much higher activity (Figure 7), indicating that the strong toluene adsorption capacity of UiO-66 and superior photocatalytic activity of TiO_2 are well inherited by $4TiO_2$@U. Besides, $4TiO_2$@U also exhibits higher desorption temperature and larger desorption peak area compared with $4TiO_2$@UN, $4TiO_2$-U-Mech and $4TiO_2$-U-Evap (Figure 11b and Table 1), suggesting that the interaction between toluene and $4TiO_2$@U is stronger than that between toluene and the other three composites. Meanwhile, $4TiO_2$@U shows higher photocatalytic performance than $4TiO_2$@UN, $4TiO_2$-U-Mech and $4TiO_2$-U-Evap (Figure S7 and S8). Thus, it can be concluded that the effective adsorption of toluene and the strong interaction between toluene and composites are beneficial to toluene degradation.

Table 1. Desorption temperature and integrated area of desorption peak of TiO_2, UiO-66 and TiO_2-UiO composite.

Samples	TiO_2	UiO-66	$4TiO_2$@U	$4TiO_2$@UN	$4TiO_2$-U-Meach	$4TiO_2$-U-Evap
Area[a]	63	4657	943	267	214	313
Temperature[b]	424	574	436	421	428	432

[a] Integrated area of desorption peak. [b] Desorption temperature.

The fast desorption of CO_2 around the active centers is also favorable for increasing catalytic activity and CO_2 selectivity. Thus, the interaction between CO_2 and materials is investigated using CO_2-TPD and the result are shown in Figure S11. Both $4TiO_2$@U and $4TiO_2$@UN present three desorption peaks at about 110, 200 and 290 °C, which can be assigned to CO_2 desorption from weak basic (50~230 °C) or strong basic (230~365 °C) groups.[24,40] As shown in Table S3, the desorption amount (the desorbed peak area) of CO_2 at strong basic sites of $4TiO_2$@UN is more than that of $4TiO_2$@U. Meanwhile, the strong base/weak base ratio of $4TiO_2$@UN is higher than that of $4TiO_2$@U. These results suggest that the adsorption capacity of $4TiO_2$@UN to CO_2 is higher than that of $4TiO_2$@U. This is because amino groups served as basic sites in the organic ligand can immobilize CO_2 molecules to stay on the reactive site.[34] Combined with the C_7H_8-TPD result, it can be found that $4TiO_2$@U can immobilize toluene for photocatalytic degradation and release CO_2 to airstream due to the higher selective adsorption of toluene than that of CO_2. Thus, $4TiO_2$@U exhibits higher photocatalytic activity and CO_2 selectivity than $4TiO_2$@UN.

2.4.2. In situ FT-IR results

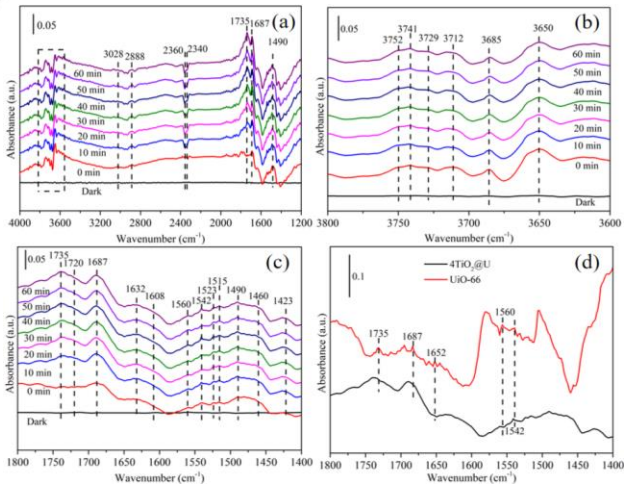

Figure 12. In situ FT-IR spectra of toluene oxidation (a) on $4TiO_2$@U, (b) and (c) at the wavenumber range of 3800-3600 and 1800-1400 cm^{-1} from Figure 13a, and (d) on UiO-66 and $4TiO_2$@U at 60 min under UV light irradiation.

In situ FT-IR tests are employed to investigate the trend of transient intermediates and give an important insight into the

reaction mechanism. Figure 12 shows in situ FTIR spectra of samples during the photo-oxidation of gas toluene in a real-time flowing system. The spectra are collected using the clean sample as the background. Prior to UV light illumination (t=0), toluene is introduced into the chamber to reach adsorption equilibrium on the surface of materials, and the characteristic peaks of toluene gradually appear. The peaks around 3028 and 2888 cm^{-1} can be ascribed to the C-H stretching vibration of the aromatic ring and methyl group,[12] respectively (Figure 12a). The abroad bands from 3800 to 3600 cm^{-1} are the feature bands of hydroxyl groups and act as the adsorption sites of toluene, including the bridged (3685 and 3650 cm^{-1}) and terminal hydroxyls (3752, 3741, 3729 and 3712 cm^{-1}) (Figure 12b).[41,42] The bands at 1608, 1515 and 1490 cm^{-1} are assigned to vibrations of the benzene rings, and the band at 1460 cm^{-1} is associated with the asymmetric methyl bending vibration (Figure 12c). When the UV light irradiates on the surface of the sample, the peaks at 2360 and 2340 cm^{-1} corresponding to CO_2 increase obviously as the reaction proceeds. Meanwhile, some new surface species are formed and increase significantly with increasing reaction time (Table S4). Specifically, the new peaks at 1687 and 1735 cm^{-1} can be attributed to the carbonyl vibration of the aldehyde group and the vibrational mode of a carbonyl group respectively, indicating the formation of benzaldehyde.[12] The bands at 1560 and 1542 cm^{-1} are caused by the asymmetric stretching vibration model of the carboxylate group COO^-, suggesting the formation of benzoic acid.[7,43] The band at 1720 and 1423 cm^{-1} reported as the v (C=O) and v (C-O) of oxalic acid, indicating toluene is effectively oxidation by composite under UV condition.[12,44] The band at 1635 cm^{-1} is related to the scissor vibration modes of physically adsorbed water. According to the experimental results and reaction pathway proposed by previous reports, toluene oxidation can be divided into three steps: 1) toluene is adsorbed on the surface of the composite; 2) the methyl groups of toluene is attacked by the active species (h^+, $\bullet O_2^-$ and •OH) and completely oxidized to carboxyl group; 3) benzoic acid breakage to generate oxalic acid and finally mineralized to CO_2 and H_2O during the reaction.[45-48]

Figure S12 displays the in situ FT-IR spectra of UiO-66 during the photo-oxidation of toluene. The feature peaks of toluene (2940, 2870, 1581 and 1506 cm^{-1}) and new peaks, such as benzaldehyde (1735, 1687, 1652 cm^{-1}), benzoic acid (1560 and 1542 cm^{-1}), oxalic acid (1720, 1698 and 1423 cm^{-1}) and CO_2 (2340 cm^{-1}), can be all clearly found. The characteristic peak intensity of intermediate products (benzaldehyde, benzoic acid) on the surface of UiO-66 at the range of 1800~1400 cm^{-1} are higher than that on $4TiO_2$@U (Figure 12d and Table S4), suggesting that the stronger adsorption affinity of intermediate products on UiO-66 surface. Meanwhile, these phenomena also can be concluded that the synergistic effect of the adsorption property of the UiO-66 and the photocatalytic activity of TiO_2 for toluene significantly enhanced the photocatalytic activity, thus avoiding the deposition of recalcitrant degradation intermediates (carbonaceous residues). Besides, some studies have pointed out that benzoic acid strongly adsorbs on the surface of the catalyst, leading to the deactivation of photocatalyst.[43] Thus, UiO-66 exhibits poor photocatalytic performance.

2.4.3. Reactive oxygen species confirmation and interfacial electron transfer

To explore the main active species and possible reaction mechanism, a series of the radical trapping experiments are carried out with trapping agents of $AgNO_3$ for e^-, triethanolamine (TEOA) for h^+, p-benzoquinone (BQ) for $\bullet O_2^-$, isopropanol (IPA) for •OH. The $\bullet O_2^-$ is the main active specie because the composite nearly deactivate when it is compounded with BQ (Figure 13). The removal ratio of toluene decreases rapidly when e^- is trapped by $AgNO_3$, suggesting that e^- can be captured by O_2 to form $\bullet O_2^-$ for the further oxidation of toluene. The conversion of toluene also obviously depresses when the composite is compounded with TEOA, indicating that h^+ is one of the main radicals for toluene degradation. In contrast, • OH is not an important contributor since the photocatalytic activity decreases slightly when the composite is treated by IPA.

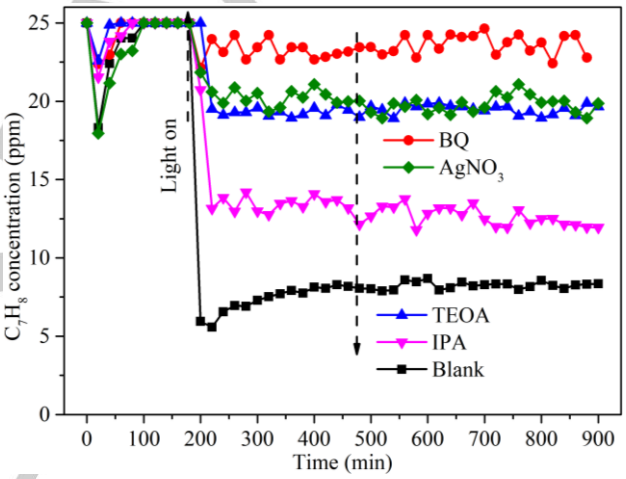

Figure 13. Photocatalytic degradation of toluene on $4TiO_2$@U composite with different kinds of scavengers.

To confirm the generation of $\bullet O_2^-$ in the reaction process, NBT is used as probe molecules to detect $\bullet O_2^-$.[49] The absorbance of NBT gradually decreases with the illumination time, suggesting that $\bullet O_2^-$ radicals are generated on the surface of $4TiO_2$@U because $\bullet O_2^-$ can react with NBT to form diformazan under light irradiation (Figure S13a). These results suggest that photoinduced electron can effectively transfer and form $\bullet O_2^-$ under light conditions, resulting in superior photocatalytic activity for organic pollutants oxidation.

Based on the experimental results above, a possible mechanism for toluene oxidation is proposed in Scheme 1. Under UV light irradiation, both TiO_2 and UiO-66 can be excited and generate electrons and holes in the conduction band (CB) and valence band (VB), respectively. Owning to the intimate interfacial contact between TiO_2 and UiO-66, the photogenerated electrons in the CB of TiO_2 can directly transfer into the VB of UiO-66. Additionally, the VB edge potential of UiO-66 and TiO_2 is higher than the oxidation potential of H_2O/• OH (2.7 eV vs NHE.). Therefore, some holes in the VB of

catalyst transform water molecule into •OH. In addition, other holes react directly with the toluene in reaction system. Meanwhile, the CB potential of UiO-66 is more negative than the potential energy of $O_2/•O_2^-$ (-0.3 eV vs. NHE),[29] thus electrons can be captured by O_2 to form $•O_2^-$. Therefore, the possible reaction formulas for the photocatalytic oxidation of toluene over TiO_2@UiO-66 composites can be described as follows:

TiO_2@UiO-66 + hv → $h^+ + e^-$

H_2O/OH^- (surface) + h^+ → •OH

$O_2 + e^- → •O_2^-$

$C_7H_8 + •O_2^-/h^+/•OH → C_6H_5CH_2• → C_6H_5CH_2OO• → C_6H_5CHO → C_6H_5COOH$

$C_6H_5COOH + •O_2^-/h^+/•OH → H_2C_2O_4 → CO_2 + H_2O$.

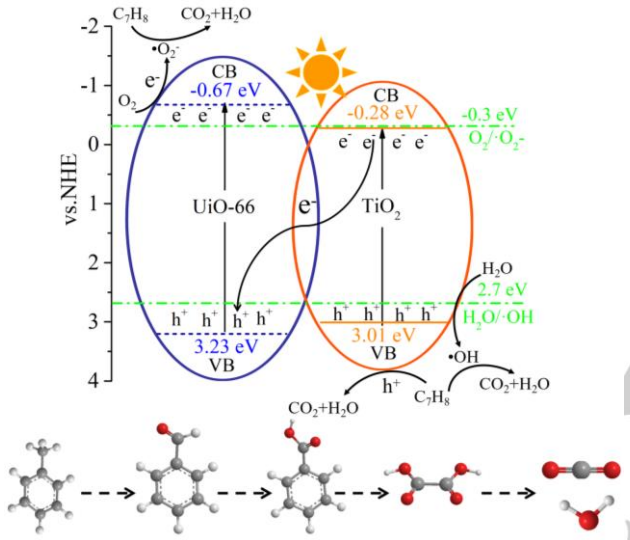

Scheme 1. The proposed mechanism for the photocatalytic oxidation of toluene on the TiO_2@UiO-66 composite.

3. Conclusion

In summary, TiO_2@UiO-66 composite has been successfully prepared by in situ solvothermal method and used for organic pollutant (toluene, formaldehyde and RhB) degradations under UV light irradiation. The TiO_2@UiO-66 composite exhibits higher photocatalytic activity for toluene and formaldehyde oxidation than TiO_2, UiO-66 and the composites prepared with evaporation and mechanical mixing methods during a 720 min of long-term evaluation under continuous flow system. The composite also exhibits outstanding RhB removal efficiency in wastewater. The improved photocatalytic activity of TiO_2@UiO-66 can be assigned to two main aspects. On one hand, the composite possesses matched band structure and close interfacial contact between UiO-66 and TiO_2, which leads to efficient separation and transfer of photoinduced carriers, thus enhancing photocatalytic activity and CO_2 selectivity. On the other hand, the synergistic effect between UiO-66 and TiO_2 in the composite combines the adsorption and photocatalytic oxidation of toluene, which not only can improve the adsorption of toluene and desorption of CO_2, but also has sufficient active sites in the composite. The mechanism for toluene oxidation implies that $•O_2^-$ and h^+ are the main active species. In situ FT-IR results reveal that the adsorbed toluene can be converted into benzaldehyde, benzoic acid and oxalic acid gradually, and decomposed into CO_2 and H_2O finally. The present work provides an effective strategy to construct a high-performance MOF based catalyst for the degradation of organic pollutants.

4. Experimental Section

4.1 Preparation of catalysts

Synthesis of TiO_2@UiO-66: TiO_2 nanoparticles were fabricated via solvothermal method.[49] TiO_2@UiO-66 composite was synthesized via the hydrothermal method. In detail, $ZrCl_4$ (0.2332 g) and H_2BDC (0.1661 g) were dissolved in 50 mL of DMF under stirring. After that, 6 mL of acetic acid was added. And then a certain amount of TiO_2 (0.80, 1.60 and 2.40 g) was dispersed into the above mixture with stirring for 30 min. The mixed solution was transferred into a 100 mL Teflon-lined stainless steel autoclave and maintained at 120 °C for 24 h without stirring. After cooling, the product was collected from the solution by centrifuging and washing with DMF and methanol as well as dried under vacuum at 100 °C for 12 h. The composite was labelled as xTiO_2@U (x=2, 4 and 6), where x is the mass ration of TiO_2 with respect to two important precursors ($ZrCl_4$ and H_2BDC) of UiO-66.

Synthesis of TiO_2@UiO-66-NH_2: Similar procedure was used in the preparation of the TiO_2@UiO-66 but using 0.1812 g NH_2-BDC instead of 0.1661 g H_2BDC. The sample was named as 4TiO_2@UN.

Synthesis of UiO-66: Similar procedure was used in the preparation of the UiO-66 except that no TiO_2 powder was added into the synthesis mixture of TiO_2@UiO-66.

Synthesis of UiO-66-NH_2: Similar procedures were used in the preparation of the UiO-66 but using 0.1812 g NH_2-BDC instead of 0.1661 g H_2BDC.

For comparison, the mechanical mixing sample was prepared by mixing the prepared 840 mg of TiO_2 and 160 mg of as-prepared UiO-66 via grinding in the air at room temperature, and it was denoted as 4TiO_2-U-Mech. Solvent evaporation sample was also prepared by mixing of the prepared 840 mg of TiO_2 and 160 mg of pristine UiO-66 in 50 mL of methanol, then stirred in fume hood until dryness and dried at 100 °C for 12 h, and it was denoted as 4TiO_2-U-Evap.

4.2. Characterizations

All the catalysts were systematically characterized by XRD, FTIR, SEM, TEM, UV-vis, XPS, PL, TPD, in situ FT-IR, photoelectrochemical measurements and detection of reactive species. The detection conditions of different characterizations are given in supporting information.

4.3. Activity test

The photocatalytic oxidation of toluene and formaldehyde were evaluated at room temperature in a continuous flow reactor.[21,50] The initial concentration of toluene and formaldehyde are 25 ppm and 10 ppm, respectively. 100 mg of samples were used for each experiment and the relative humidity was 60%.

The photocatalytic degradation of RhB was carried out in a home-made reactor.[8] 20 mg of a photocatalyst was added to 100 mL of solution containing 20 mg/L RhB.

Acknowledgements

This work was supported by National Natural Science Foundation of China (21777047) and the Scientific Research Project of Guangzhou City (201804020026).

Conflict of Interest

The authors declare no conflict of interest.

Keywords: TiO_2@UiO-66 • VOCs • photocatalytic oxidation • reaction mechanism • synergistic effect

[1] A. Chaudhary, S. Hellweg, *Environ. Sci. Technol.* **2014**, *48*, 14607-14614.
[2] D. Sarigiannis, S. P. Karakitsios, A. Gotti, I. Liakos, A. Katsoyiannis, *Environ. int.* **2011**, *37*, 743-765.
[3] H. Huang, Y. Xu, Q. Feng, D. Y. C. Leung, *Catal. Sci. Technol.* **2015**, *5*, 2649-2669.
[4] J. Fan, Q. M. Ren, S. P. Mo, Y. H. Sun, M. L. Fu, J. L. Wu, L. M. Chen, P. R. Chen, D. Q. Ye, *ChemCatChem*, **2020**, *12*, 1046-1054.
[5] S. Weon, J. Choi, T. Park, W. Choi, *Appl. Catal. B* **2017**, *205*, 386-392.
[6] S. Weon, W. Choi, *Environ. Sci. Technol.* **2016**, *50*, 2556-2563.
[7] A. H. Mamaghani, F. Haghighat, C. S. Lee, *Appl. Catal. B* **2017**, *203*, 247-269.
[8] G. Y. He, J. H. Zhang, Y. Hu, Z. G. Bai, C. H. Wei, *Appl. Catal. B* **2019**, *250*, 301-312.
[9] X. Song, Y. Hu, M. M. Zheng, C. H. Wei, Appl. Catal. B **2016**, *182*, 587-597.
[10] H. Liu, B. Shen, M. Xing, J. Zhang, B. Tian, *Res, Chem, Intermediat.* **2016**, *42*, 3459-3471.
[11] F. He, A. Y. Meng, B. Cheng, W. K. Ho, J. G. Yu, *Chinese J. Catal.* **2020**, *41*, 9-20.
[12] S. Bao, J. Wan, B. Tian, J. Zhang, *Res, Chem, Intermediat*. **2018**, *44*, 6137-6149.
[13] X. G. Wang, M. H. Sun, M. Muruganathan, Y. R. Zhang, L. Z. Zhang, *Appl. Catal. B* **2020**, *260*, 118205-118215.
[14] J. F. Qu, D. Y. Chen, N. J. Li, Q. F. Xu, H. Li, J. H. He, J. M. Lu, *Appl. Catal. B* **2019**, *256*, 117877-117884.
[15] Y. J. Xin, Q. H. Chen, G. D. Zhang, *J. Alloy. Compd.* **2018**, *751*, 231-240.
[16] X. J. Zou, X. Y. Li, Q. D. Zhao, S. M. Liu, *J. Colloid Inter. Sci.* **2012**, *383*, 13-18.
[17] P. Falcaro, R. Ricco, A. Yazdi, I. Imaz, S. Furukawa, D. Maspoch, R. Ameloot, J. D. Evans, C. J. Doonan, *Coordin. Chem. Rev*. **2016**, *307*, 237-254.
[18] D. Alezi, Y. Belmabkhout, M. Suyetin, P. M. Bhatt, L. J. Weseliński, V. Solovyeva, K. Adil, I. Spanopoulos, P. N. Trikalitis, A. Emwas, M. Eddaoudi, *J. Am. Chem. Soc.* **2015**, *137*, 13308-13318.
[19] Z. X. Zhao, X. L. Ma, A. Kasik, Z. Li, Y. S. Lin, *Ind. Eng. Chem. Res.* **2012**, *52*, 1102-1108.
[20] K. Epp, I. Luz, W. R. Heinz, A. Rapeyko, F. X. L. i. Xamena, R. A. Fischer, *ChemCatChem* **2020**, *12*, 1720-1725.
[21] J. H. Zhang, Y. Hu, J. X. Qin, Z. X. Yang, M. L. Fu, *Chem. Eng. J.* **2020**, *385*, 123814-123826.
[22] P. Z. Yao, H. L. Liu, D. T. Wang, J. Y. Chen, G. Y. Li, T. C. An, *J. Colloid Inter. Sci.* **2018**, *522*, 174-182.
[23] Z. G. Zhang, X. Li, B. Liu, Q. D. Zhao, G. Chen, *RSC adv.* **2016**, *6*, 4289-4295.
[24] J. Kim, S. N. Kim, H. G. Jang, G. Seo, W. S. Ahn, *Appl. Catal. A* **2013**, *453*, 175-180.
[25] A. Crake, K. C. Christoforidis, A. Kafizas, S. Zafeiratos, C. Petit, *Appl. Catal. B* **2017**, *210*, 131-140.
[26] X. J. Wang, X. L. Zhao, D. Q. Zhang, G. S Li, H. X. Li, *Appl. Catal. B* **2018**, *228*, 47-53.
[27] M. J. Katz, Z. J. Brown, Y. J. Colón, P. W. Siu, K. A. Scheidt, R. Q. Snurr, J. T. Hupp, O. K. Farha, *Chem. Commun.* **2013**, *49*, 9449-9451.
[28] X. Liu, R. Dang, W. J. Dong, X. B. Huang, J. Tang, H. Y. Gao, G. Wang, *Appl. Catal. B* **2017**, *209*: 506-513.
[29] X. Q. Xu, R. X. Liu, Y. H. Cui, X. X. Liang, C. Lei, S. Y. Meng, Y. L. Ma, Z. Q. Lei, Z. W. Yang, *Appl. Catal. B* **2017**, *210*, 484-494.
[30] X. D. Zhang, Y. Yang, X. T. Lv, Y. X. Wang, N. Liu, D. Chen, L. F. Cui, *J. Hazard. Mater.* **2019**, *366*, 140-150.
[31] T. Lee, Y. H. Chang, H. L. Lee, *CrystEngComm*, **2017**, *19*, 426-441.
[32] A. A. Silahua-Pavón, C. G. Espinosa-González, F. Ortiz-Chi, J. GpePacheco-Sosa, H. Pérez-Vidal, J. CarlosArévalo-Pérez, S. Godavarthi, J. G. Torres-Torres, *Catal. Commun.* **2019**, *129*: 105723.
[33] Y. Su, Z. Zhang, H. Liu, Y. Wang, *Appl. Catal. B* **2017**, *200*, 448-457.
[34] S. Z. You, Y. Hu, X. C. Liu, C. H. Wei, *Appl. Catal. B* **2018**, *232*, 288-298.
[35] Y. C. Huang, B. Long, M. N. Tang, Z. B. Rui, M. S. Balogun, Y. X. Tong, H. B. Ji, *Appl. Catal. B* **2016**, *181*, 779-787.
[36] D. R. Sun, Y. H. Fu, W. J. Liu, L. Ye, D. K. Wang, L. Yang, X. Z. Fu, Z. H. Li, *Chem-Eur. J.* **2013**, *19*, 14279-14285.
[37] A. H. Mamaghani, F. Haghighat, C. S. Lee, *Build. Environ.* **2018**, *138*, 275-282.
[38] Q. J. Geng, Q. M. Wang, B. Zhang. *Ind. Eng. Chem. Res.* **2012**, *51*, 15360-15373.
[39] O. Debono, F. Thevenet, P. Gravejat, V. Hequet, C. Raillard, L. Lecoq, N. Locoge, *Appl. Catal. B* **2011**, *106*, 600-608.
[40] G. Y. Jiang, L. Zhang, Z. Zhao, X. Y. Zhou, A. J. Duan, C. M. Xu, J. S. Gao, *Appl. Catal. A* **2008**, *340*, 176-182.
[41] M. El-Roz, M. Kus, P. Cool, F. Thibault-Starzyk, *J. Phys. Chem. C*. **2012**, *116*, 13252-13263.
[42] J. J. Sun, X. Y. Li, Q. D. Zhao, M. O. Tadé, S. M. Liu, *J. Mater. Chem. A*. **2015**, *3*, 21655-21663.
[43] M. D. Hernández-Alonso, I. Tejedor-Tejedor, J. M. Coronado, M. A. Anderson, *Appl. Catal. B* **2011**, *101*, 283-293.
[44] J. Liu, P. L. Wang, W. Q. Qu, H. R. Li, L. Y. Shi, D. S. Zhang, *Appl. Catal. B* **2019**, *257*, 117880-117888.
[45] W. Cui, J. Y. Li, L. Chen, X. A. Dong, H. Wang, J. P. Sheng, Y. J. Sun, Y. Zhou, F. Dong, *Sci. Bull.* **2020**, *65*, 1626-1634.
[46] R. M. Chen, J. Y. Li, J. P. Sheng, W. Cui, X. A. Dong, P. Chen, H. Wang, Y. J. Sun, F. Dong, *Appl. Catal. B* **2020**, *278*, 119318.
[47] F. Zhang, X. Y. Li, Q. D. Zhao, Q. Z. Zhang, M. Tadé, S. M. Liu, *J. Colloid Inter. Sci.* **2015**, *457*, 18-26.
[48] J. Y. Li, R. M. Chen, W. Cui, X. A. Dong, H. Wang, K. H. Kim, Y. H. Chu, J. P. Sheng, Y. J. Sun, F. Dong, *ACS Catal.* **2020**, *10(13)*, 7230-7239.
[49] J. X. Qin, J. Wang, J. J. Yang, Y. Hu, M. L. Fu, D. Q. Ye, *Appl. Catal. B* **2020**, *267*, 118667-118676.
[50] Q. Q. Huang, Y. Hu, Y. Pei, J. H. Zhang, M. L. Fu, *Appl. Catal.* **2019**, *259*, 118106-118119.

Entry for the Table of Contents

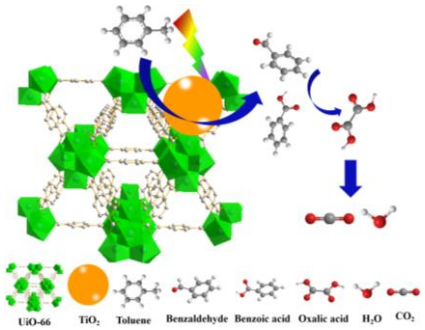

TiO_2@UiO-66 composite synthesized by one-pot solvent-thermal method possesses the characteristic of tight contact interface and matched band structure between TiO_2 and UiO-66, which are conducive to the separation and transfer of charge carriers, thus promoting the degradation of adsorbed toluene on UiO-66.